Combustion and Flame 160 (2013) 1870–1875

Contents lists available at SciVerse ScienceDirect

Combustion and Flame

journal homepage: www.elsevier.com/locate/combustflame

# Pyrophoricity of nascent and passivated aluminum particles at nano-scales

Dilip Srinivas Sundaram, Puneesh Puri [1], Vigor Yang *

*School of Aerospace Engineering, Georgia Institute of Technology, Atlanta, GA 30332, USA*

ARTICLE INFO

*Article history:*
Received 1 January 2013
Received in revised form 6 March 2013
Accepted 31 March 2013
Available online 29 April 2013

*Keywords:*
Aluminum
Nano-particle
Pyrophoricity
Oxidation
Ignition

ABSTRACT

Pyrophoricity of nascent and passivated nano-aluminum particles in air is studied theoretically using energy balance analyses. The work incorporates size-dependence of physicochemical properties of particles at nano-scales, and considers free-molecular and radiation heat exchange with the surrounding environment. The heterogeneous oxidation process is modeled using the Mott–Cabrera mechanism. Nascent aluminum particles with diameters lower than 32 nm are predicted to be pyrophoric. The critical diameter for particles passivated with 0.3-nm thick oxide layer is calculated as 3.8 nm. Particles with oxide layers thicker than 0.3 nm are found to be non-pyrophoric. The sensitivity analysis suggests that the model results are significantly affected by the choice of physicochemical properties, polymorphic state of the oxide layer, parameters of the Mott–Cabrera oxidation kinetics, and heat-transfer correlation. The critical particle size increases by 40%, when bulk material properties calculated at room temperature are used and the oxide layer is assumed to be in a crystalline form. It decreases by 43%, when free-molecular effects are neglected.



## 1. Introduction

Aluminum particles are extensively used in propulsion and energy-conversion applications due to their high oxidation enthalpy, relative safety, and low cost [1]. When a nascent aluminum particle is exposed to an oxidizing environment at room temperature, the chemical reactions between the aluminum atoms and oxidizer molecules result in the formation of an amorphous aluminum oxide ($Al_2O_3$) layer on the particle surface [2]. Typically, the rate of heat-release due to these chemical reactions is lower than that of heat loss to the surrounding environment. As a result, the particle does not ignite and the thickness of the oxide layer saturates at a value in the range of 0.5–4 nm, depending on the temperature and duration of exposure to the oxidizing gas [2]. The oxide layer protects the aluminum core from further attack of the oxidizer molecules. The ignition temperature of passivated aluminum particles decreases from 2350 K (melting point of the oxide layer) at 100 μm to 933 K (melting point of the aluminum core) at 0.1 μm [3]. The enhanced reactivity of nano-sized particles poses significant safety hazards. If the size of the particle is decreased below a critical value, the particle could ignite when exposed to an oxidizing gas at room temperature, a phenomenon known as pyrophoricity [4]. It is a major safety issue during particle manufacture, handling, and storage. It can also be employed for useful applications like decoy flare for defending heat-seeking missiles [5]. Reliable measurements or predictions of the critical particle size for pyrophoricity are of paramount interest.

Theoretical studies on metal pyrophoricity are very limited. Glassman et al. [4] postulated that a metal particle is pyrophoric if the chemical energy release is sufficient to vaporize the metal. A quasi steady-state energy balance was performed. For an oxide-layer thickness of 2.5 nm, the critical particle diameter was calculated to be 23 nm. The study ignored the effect of heat losses to the ambient environment and considered bulk material properties. For nano-sized particles, the melting and boiling points [6–12], heat of fusion [9–12], vapor pressure [13–15], ignition temperature [3], and heat of reaction [16] are substantially different from their respective bulk values. Puri [17] estimated the critical particle size by performing transient energy balance in conjunction with the use of size-dependent thermophysical properties. The oxidation was assumed to be controlled by diffusion of oxygen molecules through the gas-phase mixture to the particle surface. The estimated critical particle size is 20 nm. It is worth noting that once a monomolecular oxide layer is formed, the oxidation of nano-aluminum particles is governed by the Mott–Cabrera oxidation kinetics [18,19]. An essential feature of this model is that the metal electrons transverse the thin oxide layer either by

* Corresponding author. Fax: +1 404 894 2760.
*E-mail address:* vigor.yang@aerospace.gatech.edu (V. Yang).
[1] Current address: Process Technology Development Engineer, Intel, Aloha, OR, USA.

0010-2180/$ - see front matter © 2013 The Combustion Institute. Published by Elsevier Inc. All rights reserved.
http://dx.doi.org/10.1016/j.combustflame.2013.03.031

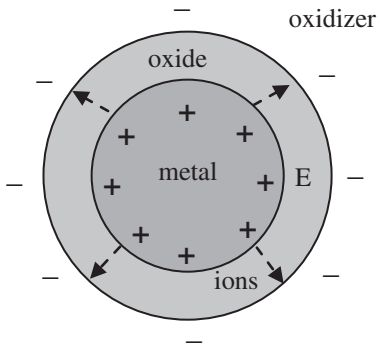


**Fig. 1.** Electric-field across the oxide layer in a spherical nano-particle surrounded by oxidizer molecules (+ positive charge, − negative charge) according to the Mott–Cabrera mechanism [19].

thermionic emission or tunneling. The electrons ionize the adsorbed oxygen atoms to create an electrostatic potential between the oxide-oxidizer and oxide–metal interfaces. Figure 1 shows the induced electric field in the particle, which significantly lowers the energy barrier for metal ion diffusion, resulting in higher oxidation rates. Recently, the Mott–Cabrera oxidation kinetics was employed to study the pyrophoricity of nascent aluminum particles [20]. The critical particle diameter was estimated to be 68 nm, which is significantly greater than the values predicted by Glassman et al. [4] and Puri [17]. The study did not consider the size dependence of physicochemical properties. The sensitivity of the results to changes in the model parameters has not been investigated. In addition, the effect of the passivating oxide layer on pyrophoricity of particles needs to be examined.

In the present study, a more comprehensive analysis is performed by taking into account transient energy balance along with accurate evaluation of physicochemical properties of nano-sized particles. The oxidation mechanism is based on a recently developed Mott–Cabrera oxidation kinetics, which is applicable for spherical nano-particles [19]. The sensitivity of the model results to the choice of physicochemical properties of the particle and gas, polymorphic state of the oxide layer, parameters of the Mott–Cabrera oxidation kinetics, and heat-transfer correlation is analyzed. Both nascent and passivated particles are considered. The temperature and pressure of the ambient environment are chosen as 300 K and 1 atm, respectively. Results from the present work are compared with those of previous theoretical and experimental studies. Reasonably good agreement with experimental data is achieved, thereby demonstrating the validity of the model.

## 2. Physicochemical properties of nano-sized aluminum particles

The physicochemical properties of nano-sized aluminum particles are significantly different from their counterparts of the bulk material [21]. The fraction of atoms on the surface layer of an aluminum particle is given by

$$f = 1 - \left(1 - \frac{2\delta}{D}\right)^3, \tag{1}$$

where $\delta$ = 286 pm and $D$ the particle diameter. It increases from 2% to 92%, when the particle size decreases from 100 to 1 nm. The surface atoms have lower coordination numbers and higher energies than the atoms in the interior of the particle, thereby leading to size-dependent properties. For example, the melting temperature of a nascent aluminum particle decreases from 937 K at 10 nm to 473 K at 2 nm [6]. The melting point, $T_m$, and the enthalpy of fusion, $L_{fus}$, of aluminum particles can be written as [12]

$$\frac{T_m(R)}{T_{m,b}} = \exp\left(-\frac{\alpha - 1}{R/R_0 - 1}\right), \tag{2}$$

$$\frac{L_{fus}(R)}{L_{fus,b}} = \frac{T_m(R)}{T_{m,b}}\left[1 - \frac{1}{(R/R_0 - 1)}\right], \tag{3}$$

where $R$ is the particle radius, $\alpha$ = 1.9186, and $R_0$ = 0.9492 nm. The subscript $b$ refers to the bulk material.

Another thermophysical property of relevance to the present study is the boiling temperature, defined as the temperature at which the vapor pressure is equal to the ambient pressure. The vapor pressure of aluminum near the surface of a liquid droplet, $p_D$, is calculated using the Kelvin equation [13]

$$p_D = p_0 \exp(4\sigma v/k_B TD). \tag{4}$$

Here $D$ is the diameter of the particle, $k_B$ the Boltzmann constant, and $v$ the molar volume. The vapor pressure of aluminum over a flat surface, $p_0$, and the surface tension of aluminum, $\sigma$, are calculated respectively as follows [14,15]:

$$p_0 = p \exp\left(13.07 - \frac{36373}{T}\right), \tag{5}$$

$$\sigma = 948 - 0.202T, \tag{6}$$

where $p$ is the pressure and $T$ the temperature. Eqs. (4)–(6) are solved iteratively to calculate the boiling temperature as a function of the particle size. Figure 2 shows the result at three different pressures of 0.5, 1, and 2 atm. The boiling temperature of aluminum increases with increasing pressure. It decreases significantly from the bulk value for particles smaller than 10 nm, a trend that is consistent with those observed for the melting temperature and enthalpy of fusion.

The heat of reaction is another physicochemical property that needs to be specified. It determines the energy release during the formation of the oxide layer on a nascent particle. The theoretical data available in Ref. [16] is curve-fitted to obtain a correlation for the heat of reaction of aluminum particles

$$\Delta H_r = -1690 + \frac{865.1}{D^{0.87}}, \tag{7}$$

where $\Delta H_r$ is the heat of reaction and $D$ the particle size in nm. The heat of reaction decreases with decreasing particle size. In other words, the oxidation reaction is less exothermic for smaller particles. This effect becomes more substantial for particles smaller than 10 nm.

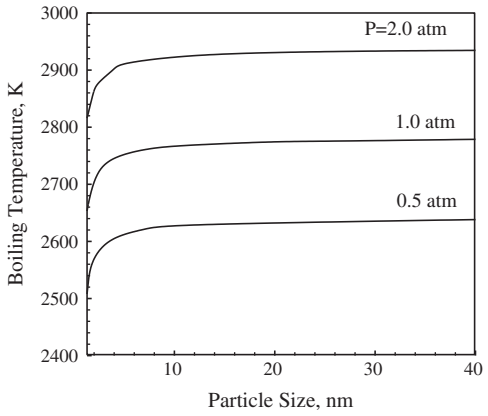


**Fig. 2.** Vaporization temperature of aluminum as a function of particle size over a pressure range of 0.5–2.0 atm.

Another parameter of concern is the density of the aluminum oxide, which exists in many metastable polymorphs. The hexagonally packed $\alpha$-$Al_2O_3$ (corundum) has a density of 4 g/cm$^3$ [2]. Other polymorphs such as $\gamma$, $\delta$, and $\theta$ phases have face-centered cubic (FCC) structures. The initial oxide layer covering the aluminum particle is amorphous [2]. The density of the amorphous oxide layer is taken to be 3.05 g/cm$^3$ [2].

## 3. Steady homogenous gas-phase reaction theory

The analysis presented in Ref. [4] assumes homogeneous gas-phase combustion of aluminum vapor and oxidizing species. It neglects heat losses to the ambient environment and size-dependence of physicochemical properties. Under these assumptions, the critical condition for metal pyrophoricity was obtained by equating the chemical heat release to the sum of the energies needed to heat the particle to its boiling point and vaporize the metal [4]:

$$\frac{(1-(\delta/R)_{cr})^3}{\left\{1-(1-(\delta/R)_{cr})^3\right\}}=\frac{\rho_{Al_2O_3}\left\{(-H^o_{ox})-\left(H^o_{T_b}-H^o_{298}\right)\right\}_{Al_2O_3}}{\rho_{Al}\left(H^o_{T_b}-H^o_{298}+L_{vap}\right)_{Al}}, \qquad (8)$$

where $\delta$ is the oxide layer thickness, $\rho$ the density, $T_b$ the boiling point of aluminum, $L_{vap}$ the enthalpy of vaporization of aluminum, and $H$ the enthalpy. The subscripts *ox* and *cr* refer to oxidation and critical condition, respectively. For the sake of comparison, bulk values of thermophysical properties are employed. They are obtained from the JANNAF tables and are given in Table 1 [22]. Figure 3 shows the calculated energy budget of the oxidation process for different particle sizes. The thickness of the oxide layer is chosen as 2.5 nm. The curves corresponding to the total absorbed and released energies intersect at a particle size of 28 nm. The predicted critical particle size agrees reasonably with the value of 28.6 nm reported in Ref. [4], thereby demonstrating the accuracy of the present calculation.

The size-dependent physicochemical properties discussed in Section 2 are used to obtain a revised estimate of the critical particle size. The density of the oxide layer is taken as 3.05 g/cm$^3$ [2]. Figure 4 shows the variation of the critical pyrophoricity ratio, $(\delta/R)_{cr}$ and particle size with the oxide layer thickness. The former decreases with increasing oxide layer thickness. For an oxide layer thickness of 2.5 nm, it takes a value of 0.217. The corresponding critical particle diameter (inclusive of the oxide layer) is 23 nm, which is lower than the value of 28 nm predicted using the constant-property assumption. The effect of pressure on the critical particle size is also studied in the range of 0.5–2 atm. Pressure plays a negligible role in the range of 0.5–2 atm. Note that the above estimates only serve as a guideline, since the analysis neglects the effects of heat losses and kinetics of oxidation of aluminum particles, as outlined in Section 1.

**Table 1**
Thermo-physical properties of bulk aluminum and alumina.

| Property | Value |
|---|---|
| Density of alumina | 4000 kg/m$^3$ |
| Density of aluminum | 2700 kg/m$^3$ |
| Heat release during oxidation, $-H^o_{298,ox}$ | 1675 kJ/mol |
| $H^o_{T_b}-H^o_{298}$ | 454 kJ/mol |
| $H^o_{T_b}-H^o_{298}+L_{vap}$ | 381.67 kJ/mol |
| Aluminum melting point | 940 K |
| Aluminum boiling point | 2740 K |
| Alumina melting point | 2327 K |
| Alumina volatilization temperature | 4000 K |

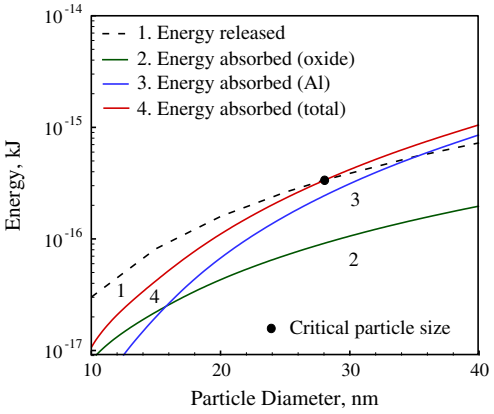


**Fig. 3.** Energy distribution for the oxidation of aluminum particles with an oxide layer thickness of 2.5 nm: steady homogeneous gas-phase reaction theory with bulk material properties.

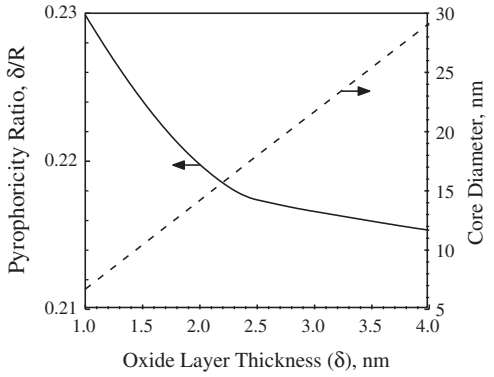


**Fig. 4.** Critical pyrophoricity ratio and core diameter as a function of the oxide layer thickness: steady homogeneous gas-phase reaction theory with size-dependent properties.

## 4. Transient heterogeneous surface reaction theory

When a nascent particle is exposed to the oxidizing gas, the temperature, oxide layer thickness, and core diameter vary continuously with time. As a result, the steady-state assumption is not valid. Particle ignition is a transient process, and the corresponding ignition delay can be characterized by the point at which temperature runaway occurs. During ignition, the rate of chemical energy release competes with that of heat loss to the oxidizing gas. An unsteady energy balance is thus required to obtain an accurate estimate of the critical particle size for pyrophoricity. The analysis follows the approach adopted by Mohan et al. [20], but is extended to include the size and temperature dependencies of particle physicochemical properties. Application of the energy conservation leads to the following equation.

$$mC_p\frac{dT}{dt}=\dot{h}_{ox}-\dot{q}_{out}, \qquad (9)$$

where $m$ is the mass of the particle, $C_p$ the specific heat of the particle, $T$ the temperature, $t$ the time, $\dot{h}_{ox}$ the rate of chemical energy release. The density and specific heat are calculated as a function of the particle temperature. The rate of heat loss to the surrounding gas, $\dot{q}_{out}$, consists of contributions from conduction and radiation, denoted by the subscripts *c* and *r*, respectively, as follows:

$$\dot{q}_{out}=\dot{q}_c+\dot{q}_r, \qquad (10)$$

In the continuum regime, the conductive heat transfer between the particle and surrounding gas is controlled by energy diffusion, given by [23]

$$\dot{q}_c = 4\pi R\lambda_g(T - T_e). \tag{11}$$

where $R$ is the particle radius and $\lambda_g$ the thermal conductivity of the gas. The subscript $e$ refers to the ambient condition. The present study concerns with large values of Knudsen number for which free-molecular effects cannot be neglected. The minimum gas temperature of concern vary between 300 K and 1500 K, depending on the particle size. The resulting Knudsen number is in the range of 10–50. As a result, the continuum heat transfer correlation ceases to be valid. In the free-molecular regime, the conductive heat-flux is replaced by the molecular heat flux, $\dot{q}_{mol}$, given by [23]:

$$\dot{q}_{mol} = \alpha\pi R^2 \frac{p_e\sqrt{8k_BT_e/\pi M}}{2}\left(\frac{\gamma^*+1}{\gamma^*-1}\right)\left(\frac{T}{T_e}-1\right), \tag{12}$$

where $M$ is the mass of the oxygen molecule, $\gamma^*$ the adiabatic constant calculated at a temperature $T^* = (T + T_e)/2$, and $\alpha = 0.85$ the accommodation coefficient [24]. The radiation heat transfer can be calculated using the Stefan–Boltzmann relation:

$$\dot{q}_r = \varepsilon A\sigma\left(T^4 - T_e^4\right), \tag{13}$$

where $A$ is the particle surface area, $\sigma$ the Stefan–Boltzmann constant, and $\varepsilon = 0.2$ the emissivity of the oxidized aluminum surface [25]. Eq. (13) is strictly not valid for nano-sized particles.

The size and temperature dependencies of the particle emissivity must be considered. Figure 5 shows the effect of particle size on the emissivity of aluminum particles at different temperatures calculated using the magnetic dipole approximation theory given in Ref. [26]. The emissivity of nano-sized aluminum is several orders of magnitude lower than its bulk value. A more accurate value of the particle emissivity can be obtained by considering the electrical dipole contribution, which may become significant at higher temperatures [27]. The analysis, however, indicates that the model results are insensitive to changes in the particle emissivity.

The heat-release term is calculated using the Mott–Cabrera oxidation kinetics [18]. Ermoline and Dreizin [19] incorporated the electric-field correction and effects of volume changes in a growing oxide layer and a shrinking aluminum core, and derived the following equations for spherical particles:

$$\frac{d\delta}{dt} = \left[(\Omega_1+\Omega_2)\left(\frac{R_c}{R}\right)^2 - \Omega_1\right] n\nu\exp\left(-\frac{W}{k_BT}\right)\exp\left(-\frac{qa\phi_M}{k_BT}\frac{R}{R_c\delta}\right),$$
$$\frac{dR_c}{dt} = \Omega_1 n\nu\exp\left(-\frac{W}{k_BT}\right)\exp\left(-\frac{qa\phi_M}{k_BT}\frac{R}{R_c\delta}\right), \tag{14}$$

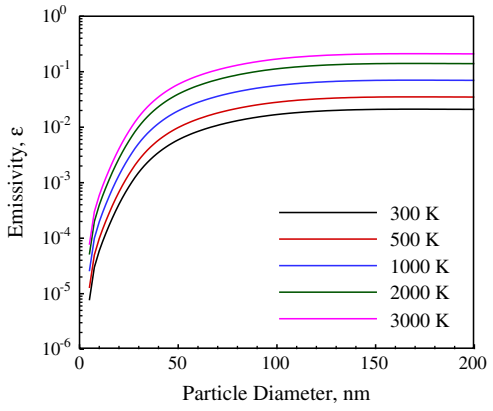


**Fig. 5.** Effect of particle size on emissivity of aluminum nano-particles at different temperatures obtained using the magnetic dipole approximation theory [26].

**Table 2**
Constants in Mott–Cabrera equations.

| Constant | Value |
|---|---|
| $n$ | 10 nm$^{-2}$ |
| $\nu$ | $10^{12}$ s$^{-1}$ |
| $a$ | 0.12 nm |
| $\phi_M$ | −1.6 V |
| $W$ | 2.6 eV |
| $q$ | 3e |
| $\Omega_1$ | −0.0166 nm$^3$ |
| $\Omega_2$ | 0.023 nm$^3$ |

where $R_c$ is the core radius and $\delta$ the oxide layer thickness. The model constants are given in Table 2. The rate of chemical heat release can be written as

$$\dot{h}_{ox} = 4\pi R_c^2\rho_{Al}h_r\frac{dR_c}{dt}, \tag{15}$$

where $h_r$ is the heat of reaction. Eqs. (14) and (15) require the presence of an oxide layer on the particle. The formation of the monomolecular oxide layer on a nascent particle is extremely fast and can be treated as an adiabatic process [20]. A detailed justification is given in Ref. [20]. Our calculations indicate that the growth of the oxide layer is adiabatic up to a thickness of 0.3 nm. This further demonstrates the validity of the assumption. As a result, chemical equilibrium analysis can be performed to calculate the particle temperature upon the formation of the 0.3-nm thick (monomolecular) oxide layer. No such calculation is necessary for passivated particles. The energy balance based on chemical equilibrium analysis can be written as

$$(m_{Al}C_{p,Al} + m_{ox}C_{p,ox})(T_f - 300) + m_{Al}L_{fus,Al} = -m_{ox}h_{ox}, \tag{16}$$

where $T_f$ is the final temperature.

## 5. Results and discussion

The theoretical framework described in Section 4 is used to analyze the pyrophoricity of nascent and passivated aluminum particles at nano-scales. Initially, the nascent particle is assumed to be devoid of the oxide layer. For passivated particles, the initial values of the oxide layer thickness in the range of 0.3–0.5 nm are considered.

### 5.1. Nascent aluminum particles

The growth of an oxide layer on a nascent aluminum particle is divided into two stages. In the first stage, a 0.3-nm thick monomolecular oxide layer is formed. As stated in Section 4, a chemical equilibrium analysis is performed to calculate the particle temperature after the formation of the oxide monolayer. A companion transient energy balance analysis employing the Mott–Cabrera kinetics is conducted to determine the minimum ignition temperature for particles encapsulated with a 0.3-nm thick oxide layer. Ignition is assumed to be achieved when the particle temperature increases monotonically beyond the melting point of the oxide film. If the ignition temperature is lower than the result of chemical equilibrium analysis, the particle can self-ignite due to heterogeneous oxidation reactions beginning at 300 K. It is, thus, considered to be pyrophoric. Figure 6 shows the variations of the temperature and oxide layer thickness with time for a particle with a core diameter of 10 nm. For an initial temperature of 680 K, the rate of chemical heat-release is not sufficient to balance the heat loss to the ambient environment. As a result, temperature runaway does not occur. The isotherm corresponds to the melting of the core at 750 K, which is lower than the bulk melting point of aluminum by 183 K. The oxide layer thickness follows a similar trend.

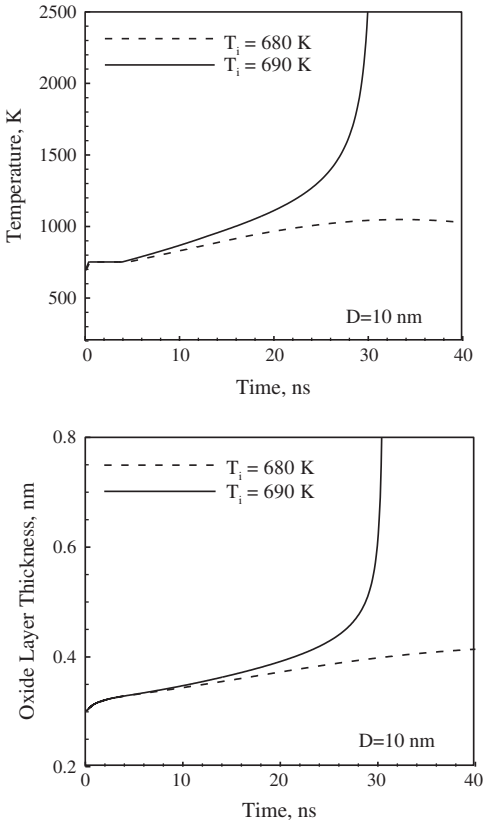


**Fig. 6.** Variations of (a) particle temperature and (b) oxide thickness with time for a core diameter of 10 nm and oxide layer thickness of 0.3 nm.

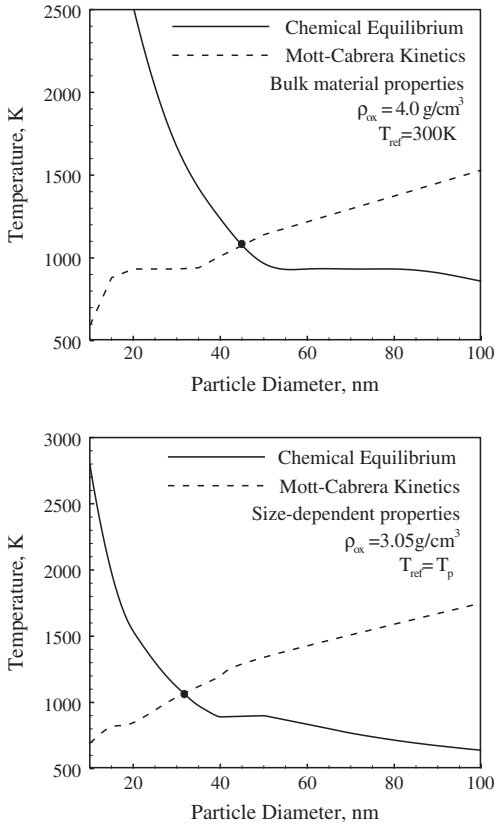


**Fig. 7.** Comparison of the particle temperature after the growth of 0.3 nm thick oxide layer and the minimum temperature necessary for ignition for (a) crystalline oxide layer and bulk material properties calculated at room temperature; (b) amorphous oxide layer with temperature and size dependent material properties.

When the initial temperature is chosen as 690 K, the temperature and oxide layer thickness increase sharply after a time period of 20 ns. The rate of chemical energy release is significantly greater than that of heat loss to the ambient environment. The same phenomenon takes place for all temperatures greater than 690 K. For a particle with a 10 nm core, the minimum ignition temperature is, thus, taken as 690 K. The sensitivity of the results to the ambient temperature stems from the fact that the reaction rate bears an exponential dependence on temperature. A similar analysis is performed for different particle sizes and the corresponding minimum ignition temperature is determined.

Figure 7 shows the comparison of the results of chemical equilibrium and transient energy balance analyses for two different cases. In the first case, bulk material properties calculated at room temperature are employed. A crystalline aluminum oxide layer with a density of 4.0 g/cm$^3$ is assumed to cover the active aluminum surface. In the second case, size and temperature dependent properties are used and an amorphous oxide layer with a density of 3.05 g/cm$^3$ is considered. The chemical equilibrium analysis indicates that the final particle temperature decreases with increasing particle size, since more energy is spent to heat a larger particle. The transient energy balance analysis, on the other hand, suggests that the minimum ignition temperature increases with increasing particle size, since the rate of heat loss to the oxidizing gas is proportional to the particle surface area. The plateau-like feature indicates that the corresponding particles need to be preheated to the melting point of the core. These two curves intersect at the critical particle size, the specific value of which is different for the two cases. For the first case, the calculated value is 45 nm, which is comparable with the estimate reported in Ref. [20]. Note that a transition-regime heat transfer model was employed in the referenced study. For the second case, the critical particle size is predicted to be 32 nm. The model results were sensitive to the changes in the parameters of the Mott–Cabrera oxidation kinetics. For example, increasing the Mott potential from 1.6 to 1.75 V resulted in an increase in the critical particle size by 18%. In the above analyses, the free-molecular regime heat transfer model is employed. Figure 8 shows the result when the continuum hypothesis is invoked. It overestimates the heat losses to the ambient environment. As a result, particles need to be heated to higher temperatures for ignition to occur. The calculated critical particle size of 18 nm is significantly lower than the value obtained using the model for the free-molecular regime. The continuum heat transfer correlation gives inadequate description of ignition and combustion of nano-sized particles. Table 3 shows the comparison between the predictions of different models and experimental data. Results from the present analysis exhibit reasonably good agreement with measurements.

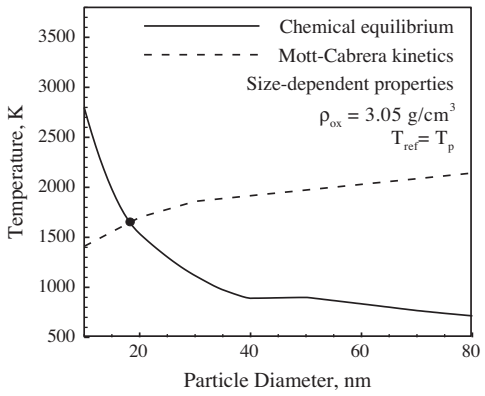


**Fig. 8.** Critical particle size predicted using the continuum heat transfer correlation.

**Table 3**
Critical particle size predicted by different models and their comparison with the experimental data.

| Model | Critical particle size (nm) |
|---|---|
| *Steady-state, homogeneous gasphase reaction theory* | |
| Constant properties [4] | 23 |
| Size-dependent properties | 18 |
| *Transient heterogeneous surface reaction theory* | |
| Diffusion oxidation model [17] | 20 |
| *Mott–Cabrera kinetics* | |
| Free molecular | 32 |
| Continuum | 18 |
| Experimental data [4] | 30 |

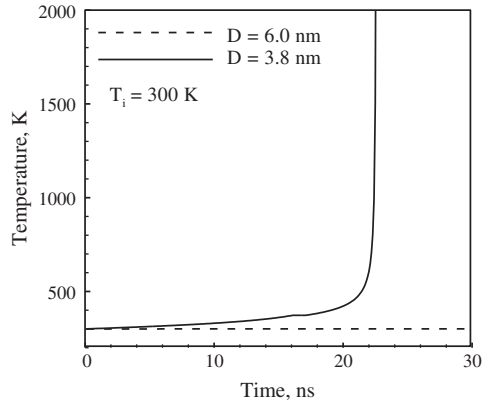


**Fig. 9.** Variation of particle temperature with time for core diameters of 3.8 and 6 nm and oxide layer thickness of 0.3 nm.

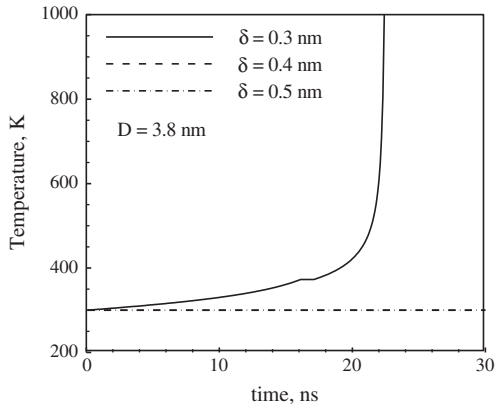


**Fig. 10.** Variation of particle temperature with time for a core diameter of 3.8 nm and oxide layer thickness of 0.3, 0.4, and 0.5 nm.

### 5.2. Passivated aluminum particles

The same approach outlined in Section 4 is adopted for passivated aluminum particles, except that the chemical equilibrium analysis is not employed. The oxide layer thickness is varied in the range of 0.3–0.5 nm. Figure 9 shows the temporal evolution of the temperature for particles with a core diameter of 3.8 and 6 nm along with an oxide layer thickness of 0.3 nm. At 300 K, temperature runaway is observed only when the particle size is 3.8 nm and, thus, the critical particle size is 3.8 nm. Figure 10 shows the temperature evolution for a core diameter of 3.8 nm and shell thickness in the range of 0.3–0.5 nm. Particles with 0.4 and 0.5 nm thick oxide layers remain stable at 300 K, suggesting that oxide layers thicker than 0.3 nm render the particle to be non-pyrophoric. Aluminum particles are typically covered by an oxide layer, which can have thickness in the range of 0.5–4 nm [2]. Moreover, particles smaller than 3.8 nm are not of practical interest. As a result, commercially available passivated particles are found to be non-pyrophoric.

## 6. Conclusions

Pyrophoricity of nano-sized nascent and passivated aluminum particles in air was studied based on a transient energy balance analysis. The work considered radiation and molecular heat exchange with the surrounding environment and employed the Mott–Cabrera oxidation mechanism for the heterogeneous chemical reactions that occur on the particle surface. The size-dependence of physicochemical properties of the particle is also incorporated. Results suggested that nascent aluminum particles with diameters lower than 32 nm are pyrophoric. The critical particle size for particles passivated with a 0.3 nm thick oxide layer was calculated as 3.8 nm. Commercially available nano-scale aluminum particles with an oxide-layer thickness in the range of 0.5–4.0 nm were predicted to be non-pyrophoric. The model results were sensitive to the choice of physicochemical properties, the Mott–Cabrera oxidation parameters, and the polymorphic state of the oxide layer. The continuum hypothesis gave inadequate description of pyrophoricity of aluminum particles at nano-scales.

## Acknowledgments

This work was sponsored by the Air Force Office of Scientific Research under Contract No. FA-9550-11-1-0002. The support and encouragement provided by Dr. Mitat A. Birkan is gratefully acknowledged.

## References

[1] E.W. Price, R.K. Sigman, in: V. Yang, T.B. Brill, W.Z. Ren (Eds.), Solid Propellant Chemistry, Combustion, and Motor Interior Ballistics, Progress in Astronautics and Aeronautics, AIAA, vol. 185, 2000, pp. 663–687.
[2] M.A. Trunov, M. Schoenitz, E.L. Dreizin, Combust. Theory Modell. 10 (2006) 604–623.
[3] Y. Huang, G.A. Risha, V. Yang, R.A. Yetter, Combust. Flame 156 (2009) 5–13.
[4] I. Glassman, P. Papas, K. Brezinsky, Combust. Sci. Technol. 83 (1992) 161–165.
[5] V. Yang, T.B. Brill, W.Z. Ren (Eds.), Solid Propellant Chemistry, Combustion, and Motor Interior Ballistics, Progress in Astronautics and Aeronautics, AIAA, vol. 185, 2000.
[6] P. Puri, V. Yang, J. Phys. Chem. C 111 (2007) 11776–11783.
[7] J. Eckert, J.C. Holzer, C.C. Ahn, Z. Fu, W.L. Johnson, Nanostruct. Mater. 2 (1993) 407–413.
[8] P. Puri, V. Yang, J. Nanopart. Res. 11 (2009) 1117–1127.
[9] P. Puri, V. Yang, J. Nanopart. Res. 12 (2010) 2989–3002.
[10] L.H. Liang, J.C. Li, Q. Jiang, Phys. B 334 (2003) 49–53.
[11] M. Zhao, Q. Jiang, Solid State Commun. 130 (2004) 37–39.
[12] Z. Zhang, X.X. Lu, Q. Jiang, Phys. B 270 (1999) 249–254.
[13] S. Panda, S.E. Pratsinis, Nanostruct. Mater. 5 (1995) 755–767.
[14] R. Hultgren, P.D. Desai, D.T. Hawkins, M. Gleiser, K.K. Kelley, Selected Values of Thermodynamic Properties of the Elements, American Society for Metals, eighth ed., Metal Parks, Ohio, 1973.
[15] S.K. Rhee, J. Am. Ceram. Soc. 53 (1970) 386–389.
[16] S.W. Chung, E.A. Guliants, C.E. Bunker, P.A. Jelliss, S.W. Buckner, J. Phys. Chem. Solids 72 (2011) 719–724.
[17] P. Puri, Ph.D. Thesis, The Pennsylvania State University, 2008.
[18] L.P.H. Jeurgens, W.G. Sloof, F.D. Tichelaar, E.J. Mittemeijer, J. Appl. Phys. 92 (2002) 1649–1656.
[19] A. Ermoline, E.L. Dreizin, Chem. Phys. Lett. 505 (2011) 47–50.
[20] S. Mohan, A. Ermoline, E.L. Dreizin, J. Nanopart. Res. 14 (2012) 723–729.
[21] K.J. Klabunde, J. Stark, O. Koper, C. Mohs, D.G. Park, S. Decker, Y. Jiang, I. Lagadic, D. Zhang, J. Phys. Chem. 100 (1996) 12142–12153.
[22] JANAF Thermodynamic Tables, third ed., American Chemical Society, 1981.
[23] A.V. Filippov, D.E. Rosner, Int. J. Heat Mass Transfer 43 (2000) 127–138.
[24] S.C. Saxena, R.K. Joshi, Thermal Accommodation and Absorption Coefficient of Gases, Hemisphere, New York, 1989.
[25] D.R. Lide, Handbook of Chemistry and Physics, CRC Press, New York, 2003.
[26] Y.V. Martynenko, L.I. Ognev, Tech. Phys. 50 (2005) 1522–1524.
[27] M. Rosenberg, R.D. Smirnov, A.Y. Pigarov, J. Phys. D: Appl. Phys. 41 (2008) 015202.